Absorption Enhancement of an Electric Quadrupole Transition of Cesium Atoms in an Evanescent Field

Satoshi Tojo, Masahiro Hasuo, and Takashi Fujimoto

Department of Engineering Physics and Mechanics, Graduate School of Engineering, Kyoto University, Kyoto 606-8501, Japan

(Received 13 April 2003; published 5 February 2004)

We have observed for the first time reflection spectra of an electric quadrupole transition for the cesium atom ($6\,^2S_{1/2}$-$5\,^2D_{5/2}$) line at an angle of incidence from $\theta_c - 11.9$ to $\theta_c + 107.5$ mrad, where θ_c is the critical angle for total reflection. From a comparison with the calculated absorption in the attenuated total reflection, the oscillator strengths for s and p polarizations were found to increase with an increase in the angle of incidence by a factor up to 1.5 at $\theta_c + 83.8$ mrad and 2.4 at $\theta_c + 107.5$ mrad, respectively, in the experiment. The dependences of the observed enhancement on the angle of incidence were in good agreement with the calculated ones for the oscillator strength of the quadrupole transition in the evanescent light.

DOI: 10.1103/PhysRevLett.92.053001 PACS numbers: 32.30.Jc, 42.62.Fi

Observation of total reflection of light at a dielectric/vapor interface is known to be a powerful spectroscopic tool to investigate atoms near the surface [1–6]. The reflected light is attenuated by vapor atoms absorbing the evanescent light which penetrates into the vapor by a few wavelengths from the surface. In the pioneering work by Boissel and Kerherve [1], absorption spectroscopy with total reflection has been demonstrated with electric dipole (E1) transitions of sodium atoms. There have been many studies on the total reflection spectroscopy in electric dipole (E1) transitions [2–8].

It is well known that the evanescent light is of an inhomogeneous nature having a wave vector $\mathbf{k} = (k_x, k_y, k_z) = (n_1 k_0 \sin\theta_i, 0, ik_0\sqrt{n_1^2\sin^2\theta_i - n_2^2})$, where k_0 is the wave number of the propagating (homogeneous) light in free space, θ_i is the angle of incidence, and n_1 and n_2 are the refractive indices of the optically denser and less dense mediums, respectively. Here we define the x axis parallel to the surface in the incident plane and the z axis perpendicular to the surface. The real k_x, which is larger than k_0, is known as the pseudomomentum and the imaginary k_z leads to a short penetration depth of the order of the light wavelength [4]. Since the interaction area of atoms with the evanescent field is appreciably smaller than that in free space, it is extremely difficult to observe an attenuated total reflection (ATR) spectrum for an optically thin medium. Therefore, optically forbidden transitions such as electric quadrupole (E2) transitions have been out of target of the reflection spectroscopy.

The oscillator strength of an E2 transition from an initial state $|i\rangle$ to a final state $|f\rangle$ is proportional to $|\hat{\mathbf{e}} \cdot \langle f|\mathbf{Q}|i\rangle \cdot \mathbf{k}|^2$, where $\mathbf{Q}$ is the quadrupole tensor whose component is $Q_{mn} = r_m r_n - \frac{1}{3} r^2 \delta_{mn}$ with the Kronecker symbol δ_{mn} and $\hat{\mathbf{e}}$ is the unit polarization vector of the light field [9]. The oscillator strength explicitly depends on the wave vector of the light field or the field gradient. Since the magnitude of the wave vector of the evanescent light is larger than that of the propagating light in free space, the oscillator strength may be enhanced in the evanescent field and may depend on the angle of incidence in total reflection.

In this Letter, we report the first measurement of reflection spectra of an E2 transition with a cesium vapor and the comparison of their dependence on the angle of incidence with the calculation.

Figure 1(a) shows our experimental arrangement. The light source is an external-cavity controlled diode laser (EOSI 2010), which has an output power up to 5 mW and the spectral linewidth of 1 MHz at the wavelength of 685 nm: the cesium electric quadrupole transition $6\,^2S_{1/2}(F = 4) \rightarrow 5\,^2D_{5/2}(F' = 2, 3, 4, 5, 6)$ as shown in Fig. 1(b). Here F' and F are the total angular momenta of upper and lower hyperfine structure (HFS) states, respectively. We scan the laser light frequency by sweeping the

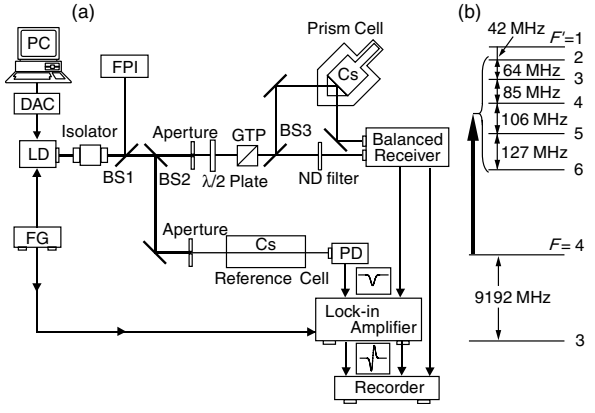

FIG. 1. (a) The experimental setup: LD, laser diode; FPI, Fabry-Pérot interferometer as a frequency marker; GTP, Glan-Thompson prism; PD, photodiode; FG, function generator; DAC, digital-analog converter; BS, beam splitter. (b) Energy level diagram of the Cs electric quadrupole transition ($6\,^2S_{1/2}$-$5\,^2D_{5/2}$) with hyperfine structure splitting.

 0031-9007/04/92(5)/053001(4)$22.50

voltage applied to the piezoelectric element which controls the external cavity. The sinusoidal voltage from a function generator is superimposed on the sweeping voltage for the purpose of frequency modulation. The modulation amplitude is 65.9 ± 0.4 MHz with the modulation frequency of 1 kHz. After passing through an optical isolator, one part of the laser light is divided by a beam splitter [BS1 in Fig. 1(a)] and incident on a Fabry-Pérot interferometer (Nihon Kagaku Eng., SA40C). The output of the interferometer is used as a frequency marker and its free spectral range is 1.870 ± 0.004 GHz.

The main part of the laser light goes through a half wave plate. By a Glan-Thompson prism, the laser light is polarized horizontally (p polarization) or vertically (s polarization). The laser beam divergence is 0.5 mrad. The intensity of the laser light is controlled by adjustment of the optical axis of the half wave plate. One-half of the main part of the laser light is incident on a prism made of quartz glass whose refractive index is 1.456 at 685 nm, giving the critical angle $\theta_c = 43.38°$ for total reflection. The intensity of the laser light beam incident on the prism is 0.10 mW/mm^2. This prism serves as one side of the cell which contains a cesium vapor. The cell, which is called the prism cell hereafter, is enclosed by a cover cell whose entrance and exit windows are wedged to eliminate the interference due to reflections at the two surfaces. The main body of the prism cell and the leg (20-mm long) connected to the cell at the opposite side to the prism are heated independently, so that the temperature of the main body are uniform and the leg serves as the coldest point which determines the vapor pressure of cesium in the cell. Throughout the measurement, temperatures of the main body and the leg of the cell are kept at 603 and 560 K, respectively, giving the cesium atom density 2.15×10^{22} m^{-3} [10]. No density anomaly is expected since the density near the surface is confirmed to be the same as that in the bulk [6]. We confirmed the experiment is free from any effects of the magnetic field caused by the heater current and the saturation caused by the laser light intensity. The angles of incidence to the prism are controlled in the range from $\theta_c - (11.9 \pm 0.3)$ to $\theta_c + (107.5 \pm 0.3)$ mrad. The reflected light and another half of the main part of the laser light are detected by a balanced detector (New focus, 2007M Nirvana Receiver). The output is lock-in detected (Princeton Applied Research, Model 5204) at the modulation frequency.

Another part of the laser light goes through a reference cell having a 100-mm long optical path. The temperature of the cell is 382 K at the coldest point, corresponding to the atom density 2.46×10^{19} m^{-3} [10]. The transmitted light is detected by a photodiode. The output signal is also lock-in detected. The transmission spectrum is used for the frequency reference of the reflection spectrum from the prism cell.

Figure 2 shows examples of the reflection spectra for both $\theta_i < \theta_c$ and $\theta_i > \theta_c$. The right figures from top to bottom are the results of averaging over 5, 5, and 20 scans,

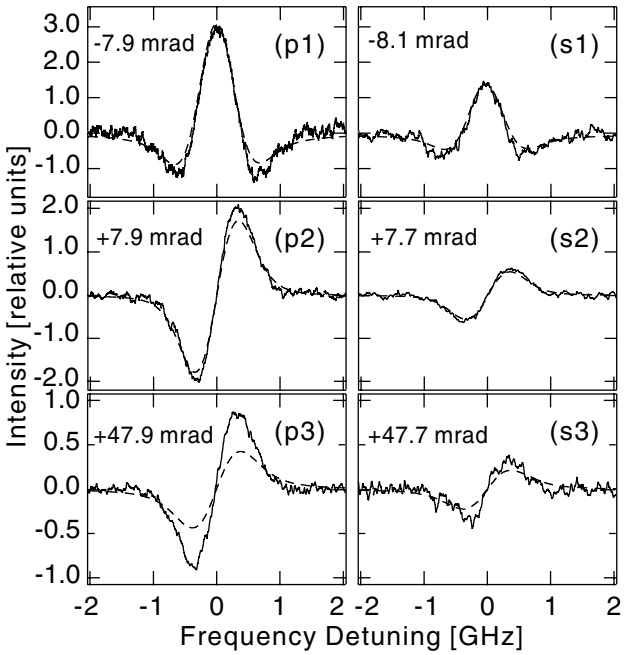

FIG. 2. Reflection spectra obtained in the experiment (solid line). The left and right figures are for p and s polarizations, respectively. The dashed line in each figure is the calculated one, in which the oscillator strength is assumed to be constant. The angular detuning is shown in each figure.

respectively, for p polarization, while the left figures are those of averaging over 3, 10, and 12 scans for s polarization. Each spectrum is the first derivative of the reflection spectrum owing to the frequency modulation technique. The HFS splittings of the excited state $6^2D_{5/2}$ are too small to be resolved in the spectrum due to the Doppler broadening of 667 MHz at 603 K. For $\theta_i < \theta_c$, the first derivative of a dispersion-type spectrum in partial reflection is seen, while for $\theta_i > \theta_c$ that of an absorption type spectrum in ATR is seen. In the case of Fig. 2 (p2), the peak absorption is 6.13×10^{-5} of the incident light intensity.

The reflection spectra are given from the Fresnel formulas as [11]

$$\mathcal{R}_{s,p}(\nu) = \left| \frac{n_1 \cos\theta_i - n_{s,p}^2 \sqrt{n_2^2 - n_1^2 \sin^2\theta_i}}{n_1 \cos\theta_i + n_{s,p}^2 \sqrt{n_2^2 - n_1^2 \sin^2\theta_i}} \right|^2, \quad (1)$$

where $n_s = 1$ for s polarization and $n_p = n_1/n_2$ for p polarization. The refractive index n_2 is related with its electric susceptibility as $n_2(\nu) = \sqrt{1 + \chi(\nu)}$.

For total reflection with an optically thin medium [in our experiment the maximum $|\chi(\nu)|$ is 3.78×10^{-6}], the reflection spectra are approximated to be [3]

$$\mathcal{R}_{s,p}(\nu) = 1 - \frac{2n_{s,p}'^2 n_1 \cos\theta_i}{n_1^2 \cos^2\theta_i + n_{s,p}''^4 (n_1^2 \sin^2\theta_i - 1)} \times \frac{\mathrm{Im}[\chi(\nu)]}{\sqrt{n_1^2 \sin^2\theta_i - 1}}, \quad (2)$$

where $n_s' = n_s'' = 1$ for s polarization, and $n_p' = n_1 \sin\theta_i$, $n_p'' = n_1$ for p polarization. The absorption spectrum is given as $S_{s,p}(\nu) = 1 - \mathcal{R}_{s,p}(\nu)$, which is proportional to $\mathrm{Im}[\chi(\nu)]$ with the θ_i-dependent proportional factor. We observed the first derivative of the absorption spectrum in the experiment. The electric susceptibility for total reflection is given as [2,3,6]

$$\chi(\nu) = \frac{Ne^2}{4\pi\epsilon_0 m_e} \sum_{F,F'} \frac{1}{\nu_{F',F}} \times \int_{-\infty}^{\infty} dv_x \int_0^{\infty} dv_z \frac{f_{F,F'} W(v_x, v_z)}{2\pi\Delta(\nu) - k_x v_x - i(\gamma - ik_z v_z)}, \quad (3)$$

where N is the atom density of the vapor, e is the elementary electric charge, ϵ_0 is the dielectric constant of vacuum, m_e is the electron mass, v_x and v_z are the respective components of atom velocity, W is the normalized Maxwell distribution function, $\Delta(\nu)$ is the detuning of the light frequency ν from the resonance $\nu_{F',F}$, and γ is the natural width. The oscillator strength distributed over HFS states is given by

$$f_{F',F} = (2F+1)(2F'+1) \begin{Bmatrix} J & I & F \\ F' & 2 & J' \end{Bmatrix}^2 f_Q, \quad (4)$$

where f_Q is the oscillator strength of an E2 transition in fine structure scheme, { } is the 6-j symbol, and J' and J are the total angular momenta of upper and lower fine structure states, respectively. The term $k_x v_x$ in the denominator of Eq. (3) is the Doppler shift with the effect of the pseudomomentum and the term $-ik_z v_z$ is the transit-time broadening. Since the profile of the absorption depends on the angle of incidence, we determine the signal amplitude in ATR spectrum by integrating over the absorption line as $A_{s,p}^{\mathrm{total}} = \int_{\mathrm{line}} S_{s,p}(\nu)\, d\nu$, which is directly proportional to the oscillator strength in an optically thin medium [see Eqs. (2) and (3)] [6]. Since $S_{s,p}(\nu)$ is a dimensionless quantity, $A_{s,p}^{\mathrm{total}}$ has a unit of Hz, which corresponds to the equivalent width of a transmission spectrum [12].

On the other hand, the electric susceptibility for partial reflection is free from the effects of the pseudomomentum and the transit-time broadening. We can express the susceptibility by using k_0 instead of k_x and omitting the term $-ik_z v_z$ in the denominator of Eq. (3) [3]. Therefore, the profile is independent of the angle of incidence. We determine the quantity $A_{s,p}^{\mathrm{part}}$, which corresponds to the signal amplitude in the ATR spectra, from the peak-to-peak intensity with the line width of the dispersion type reflection spectrum.

We determine the angular detuning δ relative to the critical angle as follows. In the vicinity of the critical angle, where angular detuning is less than 5 mrad, $A_{s,p}^{\mathrm{total}}$ and $A_{s,p}^{\mathrm{part}}$ show remarkable dependence on the angular detuning (see Fig. 3). The dependence is known to be $|\delta|^{-1/2}$ for both cases [13] [see the θ_i-dependent proportional factor in Eq. (2) for total reflection]. The experimental $A_{s,p}$ is fitted to this dependence and the critical angle is determined. The values of the angular detuning thus determined are shown in Fig. 2. A slight difference of 0.2 mrad between p and s polarizations may be due to the rotation of the Glan-Thompson prism.

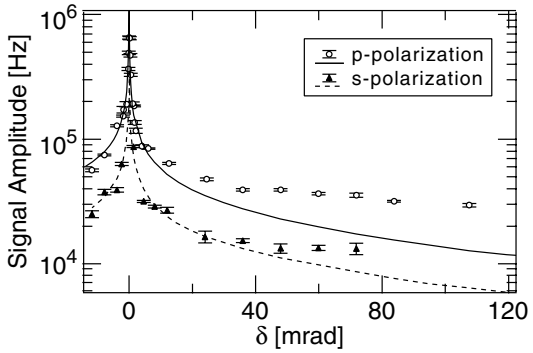

FIG. 3. Dependence of the signal amplitude on the angular detuning from the critical angle. The open circles and the closed triangles are the experimental results. The solid and dashed lines are the calculated results, where the oscillator strength is assumed to be constant.

In Fig. 2 we show the calculated spectra by the dashed lines. We use the value of the oscillator strength $f_Q = 5.65 \times 10^{-7}$ from Ref. [14] in the calculation. No adjustment is made in all the figures. Near the critical angle, the calculation is in good agreement with the experiment. The intensity ratio between p and s polarizations $(n_1/n_2)^2$ is seen in the top and middle figures. However, the reproduction becomes very poor for a large angle of incidence (bottom figures), especially for p polarization. Figure 3 shows the signal amplitude in both the experiment and the calculation. Figure 4 is another plot which shows the ratio between the experiment and the calculation. We include uncertainty of our laser beam divergence as the

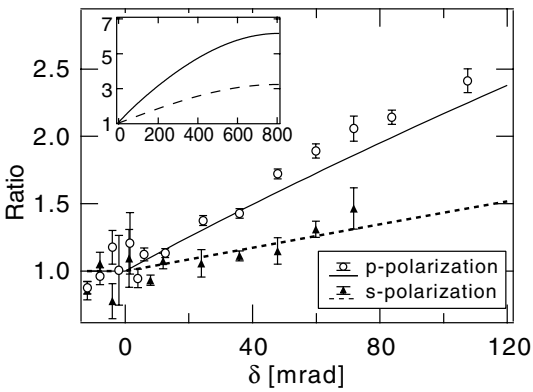

FIG. 4. The ratio of the signal amplitudes between the experiment and the calculation, as a function of the angular detuning from the critical angle. In the calculation, the oscillator strength is assumed to be constant. The solid and dashed lines show $g_p(\theta_i)$ and $g_s(\theta_i)$, respectively. In the inset $g_p(\theta_i)$ and $g_s(\theta_i)$ are shown up to $\delta = +814$ mrad, which corresponds to $\theta_i = \pi/2$ rad.

experimental uncertainties of the ratio. In Fig. 4, an increase of the ratio with the increase in the angular detuning is clearly recognized.

Thus far, we have implicitly assumed a constant oscillator strength. Now, we consider the quadrupole interaction of an atom with the evanescent field. For an alkali-metal atom, the wave function is written as $R_{nl}(r)Y_{lm}(\theta, \phi)$ with the radial function $R_{nl}(r)$ and the spherical harmonics $Y_{lm}(\theta, \phi)$, where n, l, and m are the principal, azimuthal, and magnetic quantum numbers, respectively. The oscillator strength of the $6\,^2S_{1/2}$-$5\,^2D_{5/2}$ transition in free space is written as

$$f_Q = \beta \frac{\pi m_e \nu}{\hbar} |\langle R_{52}|r^2|R_{60}\rangle|^2 \times \sum_m \left| \hat{\mathbf{e}} \cdot \left\langle Y_{2m} \left| \frac{\mathbf{Q}}{r^2} \right| Y_{00} \right\rangle \cdot \mathbf{k}_0 \right|^2, \quad (5)$$

where $\mathbf{k}_0$ is the wave vector in free space, and β is the ratio of the oscillator strength of the $6\,^2S_{1/2}$-$5\,^2D_{5/2}$ transition f_Q in the total oscillator strength of the $6S$-$5D$ transition [14]. The radial part in Eq. (5) is associated with the atomic states only, and the angular part can be regarded as the contribution of the quadrupole component of the electric field.

The polarization vector of the evanescent field for s polarization is $\hat{\mathbf{e}}_s = (0, 1, 0)$. For p polarization, the polarization is elliptical on the incident plane and the magnitude of the polarization vector $\mathbf{e}_p$ is larger than unity [11]. In this case, the evanescent light field is given as $\mathbf{e}_p E_p$, where E_p is the refracted field in the vapor obtained from the Fresnel formulas [3]. For the calculation of the oscillator strength in the evanescent field, we adopted the unit polarization vector $\hat{\mathbf{e}}_p = (\epsilon_x, \epsilon_y, \epsilon_z) = (2n_1^2\sin^2\theta_i - n_2^2)^{-1/2}(-i\sqrt{n_1^2\sin^2\theta_i - n_2^2}, 0, n_1\sin\theta_i)$ [3] because the oscillator strength corresponds to the efficiency of polarization generation by the field at the atom and is independent of the field intensity. Thus, the oscillator strengths for s polarization (f_Q^s) and p polarizations (f_Q^p) are expressed as

$$f_Q^{s,p} = \beta \frac{\pi m_e \nu}{\hbar} |\langle R_{52}|r^2|R_{60}\rangle|^2 \sum_m \left| \hat{\mathbf{e}}_{s,p} \cdot \left\langle Y_{2m} \left| \frac{\mathbf{Q}}{r^2} \right| Y_{00} \right\rangle \cdot \mathbf{k} \right|^2 = g_{s,p}(\theta_i) f_Q, \quad (6)$$

where

$$g_s(\theta_i) = 2n_1^2\sin^2\theta_i - n_2^2 = \frac{|k_x|^2 + |k_z|^2}{k_0^2}, \quad (7)$$

$$g_p(\theta_i) = \frac{8n_1^4\sin^4\theta_i - 8n_1^2\sin^2\theta_i + n_2^2 + n_2^4}{2n_1^2\sin^2\theta_i - n_2^2} = \frac{4|\epsilon_x k_x|^2 + 4|\epsilon_z k_z|^2 + 3|\epsilon_x k_z|^2 + 3|\epsilon_z k_x|^2 + 10|\epsilon_x \epsilon_z k_x k_z|}{3k_0^2}. \quad (8)$$

We call these quantities the enhancement factors. It should be noted that the enhancement factor for s polarization is directly associated with the magnitude of the wave vector or the field gradient while the factor for p polarization is associated with not only the wave vector but also the polarization vector.

The solid and dashed lines in the inset of Fig. 4 show the enhancement factors for p and s polarizations, respectively. The factor for p polarization even reaches 6 at large angles of incidence. In Fig. 4 we compare the calculated enhancement factor with the experiment. The calculated results are in good agreement with the experiment. The experimental ratio for p polarization is slightly larger than the calculated one for large angles of incidence. We do not have a positive explanation to this discrepancy at present. A possible candidate for additional enhancement may be an effect of short range interactions with the surface. Since the absorbing atoms are located very close to the solid surface, the absorption characteristics of the atoms could be further affected by interactions with the surface; e.g., the wave function mixing as in the case of the collision induced dipole transition [15]. It is noted that, if the effect of the short range interaction is substantial, the observed absorption, which is a kind of an average over the evanescent light field, may be affected only by a small amount even though the effect increases with an increase in the angle of incidence.

[1] P. Boissel and F. Kerherve, Opt. Commun. **37**, 397 (1981).
[2] S. Tojo, M. Hasuo, and T. Fujimoto, J. Phys. Soc. Jpn. **72**, 1069 (2003).
[3] G. Nienhuis, F. Schuller, and M. Ducloy, Phys. Rev. A **38**, 5197 (1988).
[4] T. Matsudo *et al.*, Phys. Rev. A **55**, 2406 (1997).
[5] M. Ducloy, in *Nanoscale Science and Technology*, edited by N. Garcia *et al.* (Kluwer, Dordrecht, 1998), p. 235.
[6] K. Zhao, Z. Wu, and H. M. Lai, J. Opt. Soc. Am. B **18**, 1904 (2001).
[7] M. Gorris-Neveux *et al.*, Opt. Commun. **134**, 85 (1997).
[8] W. Lukosz, J. Opt. Soc. Am. **69**, 1495 (1979).
[9] M. Weissbluth, *Atoms and Molecules* (Academic, San Francisco, 1978), Chap. 22, p. 497.
[10] A. N. Nesmeyanov, *Vapor Pressure of Chemical Elements* (Elsevier, Amsterdam, 1963), p. 146.
[11] M. Born and E. Wolf, *Principles of Optics* (Cambridge University Press, Cambridge, England, 1999), 7th ed., Sect. 1.5.
[12] A. Thorne, U. Litzén, and S. Johansson, *Spectrophysics* (Springer-Verlag, Berlin, 1999), Chap. 9.
[13] P. Simoneau *et al.*, Opt. Commun. **59**, 103 (1986).
[14] K. Niemax, J. Quant. Spectrosc. Radiat. Transfer **17**, 125 (1977).
[15] T. Fujimoto, K. Ueda, and K. Fukuda, J. Quant. Spectrosc. Radiat. Transfer **21**, 89 (1979).